

Keep Rollin’ – Whole-Body Motion Control and Planning for Wheeled Quadrupedal Robots

Marko Bjelonic, C. Dario Bellicoso, Yvain de Viragh, Dhionis Sako,
F. Dante Tresoldi, Fabian Jenelten and Marco Hutter

Abstract—In this paper, we show dynamic locomotion strategies for wheeled quadrupedal robots which combine the advantages of walking and driving. The developed optimization framework tightly integrates the additional degrees of freedom introduced by the wheels. Our approach relies on a Zero-Moment Point based motion optimization which continuously updates reference trajectories. The reference motions are tracked by a hierarchical whole-body controller which optimizes the generalized accelerations and contact forces by solving a sequence of prioritized tasks including the non-holonomic rolling constraints. Our approach has been tested on the torque-controllable robot ANYmal equipped with non-steerable, torque-controlled wheels. We conducted experiments on flat, inclined and rough terrain, whereby we show that integrating the wheels into the motion control and planning framework results in intuitive motion trajectories, which enable more robust and dynamic locomotion compared to other wheeled-legged robots.

I. INTRODUCTION

The invention of the wheel is one of the major technological advances of humankind. In daily life, it enables us to move faster and more efficiently compared to leg-based locomotion. However, the latter is more versatile and offers the possibility to negotiate challenging environments. Combining both strategies into one system offers great possibilities to achieve the best of both worlds. While most of the advances towards autonomous mobile robots either focus on pure walking or driving, this paper shows how to plan and control trajectories for wheeled-legged robots as depicted in Fig. 1 to achieve dynamic locomotion. We believe that such kinds of systems offer the solution for many robotic tasks as described in [1], e.g., rapid exploration, payload delivery, search and rescue, and industrial inspection.

A. Related Work

Recent years have shown an active research area which focuses on the combination of wheeled and legged locomotion. However, wheeled-legged robots like [3]–[6] are more like an active suspension system while driving and the legs are not used as a locomotion alternative to the wheels.

DRC-HUBO+ [7] is a wheeled humanoid robot which is able to switch between a walking and a driving configuration.

This work has been conducted as part of ANYmal Research, a community to advance legged robotics.

This work was supported in part by the Swiss National Science Foundation through the National Centres of Competence in Research Robotics (NCCR Robotics) and Digital Fabrication (NCCR dfab).

All authors are with the Robotic Systems Lab, ETH Zürich, 8092 Zürich, Switzerland, email: `firstname.surname@mavt.ethz.ch`

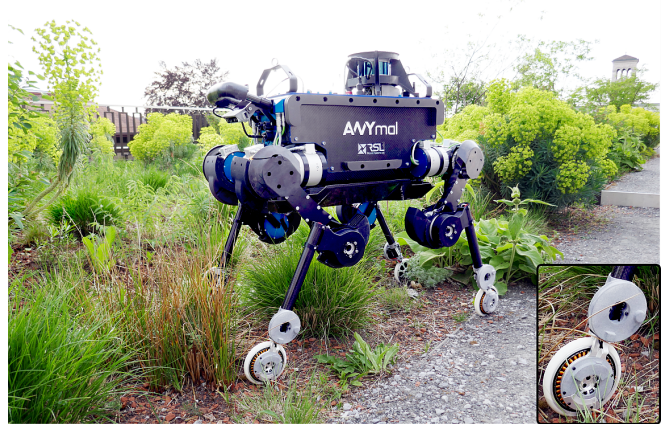


Fig. 1. The fully torque-controllable quadrupedal robot ANYmal [2] is equipped with four non-steerable, torque-controlled wheels. Thus, the number of actuated joint coordinates n_τ and the number of joints n_j are both equal to 16.

While driving, the robot is in a crouched position, and as such, the legs are not used for locomotion.

Momaro [8], on the other hand, shows driving and stepping without changing its configuration. This wheeled quadrupedal robot uses a kinematic approach to drive and to overcome obstacles like stairs and steps. Recently, the *Centauro* robot [9] showed similar results over stepping stones, steps and first attempts to overcome stairs. However, both systems show only slow static maneuvers.

There is a clear research gap for wheeled-legged robots. Most of the robots using actuated wheels are not taking into account the dynamic model of the whole-body including the wheels. The lack of a dynamic model hinders the robots to perform dynamic locomotion during walking and driving. In addition, torque control for the wheels is not explored. Without force or torque control, the friction constraints related to the no-slip condition cannot be fulfilled, and locomotion is not robust against unpredicted terrain irregularities. However, research areas in traditional legged locomotion [2], [10]–[15] offer solutions to close this gap.

So far, Boston Dynamics’ wheeled bipedal robot *Handle* [16] is the only one that demonstrated dynamic motions to overcome high obstacles while showing adaptability against unpredicted terrain irregularities. Due to the missing publications on *Handle*, there is no knowledge about Boston Dynamics’ locomotion framework.

B. Contribution

This paper shows dynamic locomotion for wheeled quadrupedal robots which combine the mobility of legs with the efficiency of driving. Our main contribution is a whole-body motion control and planning framework which takes into account the additional degrees of freedom introduced by torque-controlled wheels. The motion planner relies on an online Zero-Moment Point (ZMP) [17] optimization which continuously updates reference trajectories for the free-floating base and the wheels. These optimized motion plans are tracked by a hierarchical whole-body controller (WBC) which takes into account the nonholonomic constraints introduced by the wheels. In contrast to the related work, all joints including the wheels are torque controlled. To the best of our knowledge, this work shows the first dynamic locomotion over flat, inclined and rough terrain for a wheeled quadrupedal robot.

II. MODELLING OF WHEELED-LEGGED ROBOTS

Similar to walking robots [10], a wheeled-legged robot can be modeled as a *free-floating base* B to which the legs including the wheels as end-effectors are attached. Given a fixed *inertial frame* I (see Fig. 2), the position from frame I to B with respect to (w.r.t.) frame I and the orientation of frame B w.r.t. frame I are described by ${}^I\mathbf{r}_{IB} \in \mathbb{R}^3$ and a Hamiltonian unit quaternion \mathbf{q}_{IB} . The generalized coordinate vector \mathbf{q} and the generalized velocity vector \mathbf{u} are given by

$$\mathbf{q} = \begin{bmatrix} {}^I\mathbf{r}_{IB} \\ \mathbf{q}_{IB} \\ \mathbf{q}_j \end{bmatrix} \in SE(3) \times \mathbb{R}^{n_j}, \mathbf{u} = \begin{bmatrix} {}^I\mathbf{v}_B \\ {}^B\boldsymbol{\omega}_{IB} \\ \dot{\mathbf{q}}_j \end{bmatrix} \in \mathbb{R}^{n_u}, \quad (1)$$

where $\mathbf{q}_j \in \mathbb{R}^{n_j}$, $n_j \in \mathbb{N}$, $n_u = 6 + n_j \in \mathbb{N}$, ${}^I\mathbf{v}_B \in \mathbb{R}^3$ are the vector of joint coordinates, the number of joint coordinates, the number of generalized velocity coordinates, the linear velocity of the frame B w.r.t. the frame I , and the angular velocity from the frame I to B w.r.t. to the frame B , respectively. With this convention, the equations of motion for wheeled-legged robots are defined by

$$\mathbf{M}(\mathbf{q})\dot{\mathbf{u}} + \mathbf{h}(\mathbf{q}, \mathbf{u}) = \mathbf{S}^T \boldsymbol{\tau} + \mathbf{J}_S^T \boldsymbol{\lambda}, \quad (2)$$

where $\mathbf{M}(\mathbf{q}) \in \mathbb{R}^{n_u \times n_u}$ is the the mass matrix, $\mathbf{h}(\mathbf{q}, \mathbf{u}) \in \mathbb{R}^{n_u}$ is the vector of Coriolis, centrifugal and gravity terms, $\boldsymbol{\tau} \in \mathbb{R}^{n_\tau}$ is the generalized torque vector acting in direction of the generalized coordinate vector, $\mathbf{J}_S = [\mathbf{J}_{C_1}^T \dots \mathbf{J}_{C_{n_c}}^T]^T \in \mathbb{R}^{3n_c \times n_u}$ is the support Jacobian, with $n_c \in \mathbb{N}$ the number of limbs in contact, and $\boldsymbol{\lambda} \in \mathbb{R}^{3n_c}$ is the vector of constraint forces. The transpose of the selection matrix $\mathbf{S} = [\mathbf{0}_{n_\tau \times n_u - n_\tau} \quad \mathbb{I}_{n_\tau \times n_\tau}]$ maps the generalized torque vector $\boldsymbol{\tau}$ to the space of generalized forces, with $n_\tau \in \mathbb{N}$ the number of actuated joint coordinates.

A. Nonholonomic Rolling Constraint

In contrast to point contacts, the acceleration of the wheel-fixed contact point¹ C_i of the i -th leg does not equal zero,

¹In contrast to the wheel-fixed contact point C_i , the leg-fixed contact point C'_i does not need to have zero velocity.

i.e., ${}^I\ddot{\mathbf{r}}_{IC_i} = \mathbf{J}_{C_i}\dot{\mathbf{u}} + \dot{\mathbf{J}}_{C_i}\mathbf{u} \neq \mathbf{0}$. Given the wheel model in Fig. 2, it can be shown that the resulting contact acceleration of a wheel is defined by

$${}^I\ddot{\mathbf{r}}_{IC_i} = \mathbf{J}_{C_i}\dot{\mathbf{u}} + \dot{\mathbf{J}}_{C_i}\mathbf{u} = \mathbf{R}_{IW_i} \begin{bmatrix} 0 \\ -R\dot{\psi}_{IW'_i} \cos(\varphi_{IW'_i})(\dot{\chi}_{IW'_i} + \dot{\theta}) \\ R(\dot{\chi}_{IW'_i} + \dot{\theta})(\dot{\chi}_{IW'_i} + \dot{\theta} + \dot{\psi}_{IW'_i} \sin(\varphi_{IW'_i})) \end{bmatrix}, \quad (3)$$

where $\mathbf{R}_{IW_i} \in \mathbb{R}^{3 \times 3}$ represents the rotation matrix that projects the components of a vector from the *wheel frame* W_i to the inertial frame I , $R \in \mathbb{R}$ is the wheel radius, and $\theta_i \in \mathbb{R}$ is the joint angle of the wheel. The yaw, roll, and pitch angle of the *wheel fixed frame* W'_i w.r.t. to the inertial frame I parametrized by an intrinsic $z - x' - y'$ sequence of Euler angles are given by $\psi_{IW'_i} \in \mathbb{R}$, $\varphi_{IW'_i} \in \mathbb{R}$, and $\chi_{IW'_i} \in \mathbb{R}$, respectively. By setting $\varphi_{IW'_i} \equiv 0$ and $\psi_{IW'_i} \equiv 0$, we obtain the acceleration for the planar case, i.e., ${}^I\ddot{\mathbf{r}}_{IC_i} = \mathbf{R}_{IW_i}[0 \ 0 \ R(\dot{\chi}_{IW'_i} + \dot{\theta})^2]^T$, which is equal to the centripetal acceleration.

B. Terrain and Contact Point Estimation

The robot is blindly locomoting on a terrain which is locally modeled using a three-dimensional plane. In an intermediate step, the terrain normal is estimated by fitting a plane through the most recent contact locations of the wheel frame W in Fig. 2 using a least-squares method as described in [12]. Given the resulting terrain normal \mathbf{n} , the estimated plane is moved along the terrain normal to the contact position C as shown in Fig. 2, i.e., the terrain plane is shifted by $\pi_{W_{x,z}}(-\mathbf{n})R/|\pi_{W_{x,z}}(-\mathbf{n})|$, where $\pi_{W_{x,z}}(-\mathbf{n})$ is the projection of the negative normal vector \mathbf{n} onto the plane spanned by \mathbf{w}_x and \mathbf{w}_z . Finally, the plane through the contact points represents the estimated terrain plane used for control and planning.

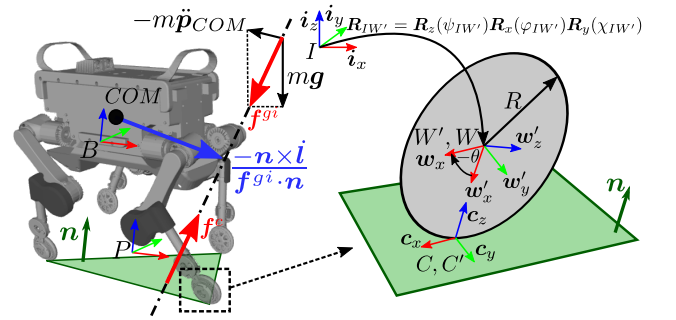


Fig. 2. The figure shows a sketch of the wheeled quadrupedal robot ANYmal and the wheel model used to derive the rolling constraint (3). As discussed in [10], we define a plan frame P which is used as a reference frame in our motion planner. In addition, the left part of the figure shows a sketch of the 3D ZMP model described in Section III-C.3. Our wheel model is based on the leg-fixed wheel frame W' which does not rotate with the wheel angle θ , the wheel frame W which rotates with the wheel angle θ , a leg-fixed contact frame C' , and a wheel-fixed contact frame C . Both contact frames are aligned with the local estimation of the terrain normal \mathbf{n} and the rolling direction of the wheel.

As illustrated in Fig. 2, the *leg-fixed contact frame*² C'_i and *wheel-fixed contact frame*³ C_i of each leg i are defined to lie at the intersection of the wheel plane with the estimated terrain plane. The contact frame's z-axis is aligned with the estimated terrain normal and its x-axis is perpendicular to the estimated terrain normal and aligned with the rolling direction⁴ c_x of the wheel.

As discussed in earlier works [10], the motion plans in Section III are computed in the *plan frame* P whose z-axis is aligned with the estimated terrain normal and whose x-axis is perpendicular to the estimated terrain normal and aligned with the heading direction of the robot. As depicted in Fig. 2, the plan frame is located at the footprint center projected onto the local terrain along the terrain normal.

III. MOTION PLANNING

The dynamic model of a wheeled-legged robot (11) includes significant nonlinearities to be handled by the motion planner. Due to this complexity, the optimization problem becomes prone to local minima and can hardly be solved in real-time on-board [13]. To overcome these problems, we simplify the system dynamics to a 3D ZMP model for motion planning [10], [18].

Fig. 3 gives an overview of the entire whole-body motion control and planning framework. The foothold optimizer, motion optimizer, and WBC modules are solving separate optimization problems in parallel such that there is no interruption between them [10]. We generate all motions plans w.r.t. the plan frame P which is defined in Section II-B. In the following, we describe the different modules.

A. Contact Scheduler

The contact schedule defines periodic sequences of lift-off and touch-down events for each leg. Based on a gait pattern library, each gait predefines the timings for each leg over a stride. Fig. 3 illustrates the gait pattern for a trotting gait. With this formulation, driving is defined by a gait pattern where each leg is scheduled to stay in contact, and no lift-off events are set.

B. Foothold Optimizer

Given a desired reference velocity of the base $v_B^{ref} = [v_{B,x}^{ref} \ v_{B,y}^{ref} \ 0]^T$ and $\omega_B^{ref} = [0 \ 0 \ \omega_{B,z}^{ref}]^T$, and the contact schedule, desired footholds⁵ are generated for each leg. Based on the contact schedule and footholds, a sequence of support polygons are generated, where each polygon defines the convex hull of expected footholds (green area in Fig. 2), as well as its time duration in seconds.

²The leg-fixed contact frame C'_i is defined as a point w.r.t. the leg-fixed wheel frame W'_i . It follows that the Jacobian $J_{C'_i}$ does not depend on the joint angle θ_i of the i -th wheel.

³The wheel-fixed contact frame C_i is defined as a point w.r.t. the wheel frame W_i . It follows that the Jacobian J_{C_i} depends on the joint angle θ_i of the i -th wheel.

⁴The rolling direction is computed by $c_x = w_y \times n / |w_y \times n|$.

⁵A foothold is the contact position C of a grounded leg.

While walking, we formulate a quadratic programming (QP) problem which optimizes over the x and y coordinates of each leg's foothold [10]. Costs are added to the QP problem which penalize the distance between the optimized foothold locations and different contributions to the computation of the footholds. We assign default foothold positions which define the standing configuration of the robot. Footholds are projected using the high-level reference velocity and assuming constant reference velocity over the duration of the optimization horizon. To ensure smoothness of the footholds, we penalize the deviation from previously computed footholds. Finally, we rely on an inverted pendulum model to stabilize the motion [12]. Inequality constraints are added to avoid collisions of the feet and to respect the maximum kinematic extension of each leg. Given the previous stance leg position and the optimized foothold, a swing trajectory for each leg is generated by fitting a spline between both positions.

Traditional legged locomotion is based on the constraint that the leg-fixed contact point C' remains stationary when in contact with the environment. In contrast, wheeled-legged robots are capable of executing trajectories along the rolling direction c_x of the wheel. This can be seen as a moving foothold. While driving, the desired leg-fixed contact position $I\dot{r}_{IC'_i}^d \in \mathbb{R}^3$, velocity $I\dot{r}_{IC'_i}^d \in \mathbb{R}^3$ and acceleration $I\ddot{r}_{IC'_i}^d \in \mathbb{R}^3$ of leg i are computed based on the reference velocities

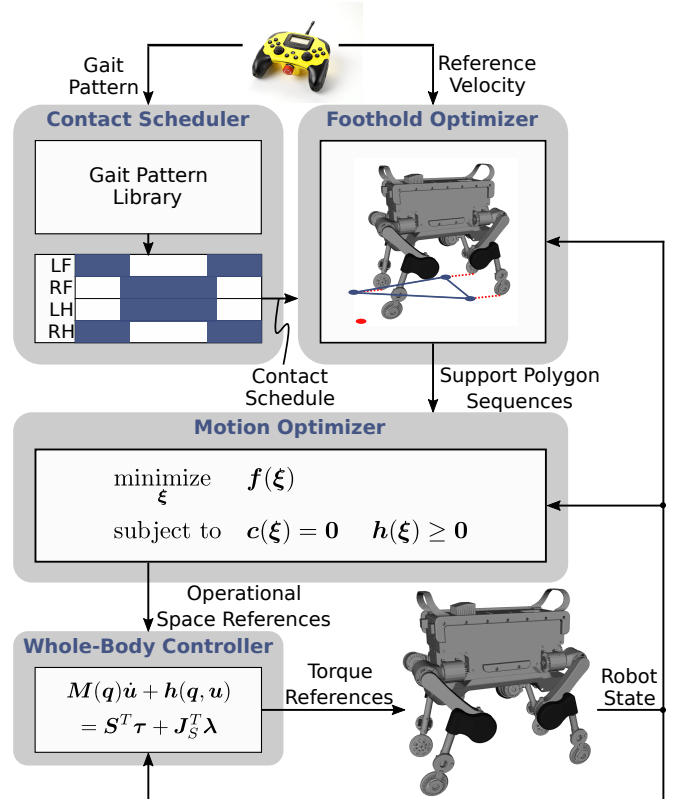


Fig. 3. The motion planner is based on a 3D ZMP approach which takes into account the support polygon sequence and the state of the robot. The hierarchical WBC which optimizes the whole-body accelerations and contact forces tracks the operational space references. Finally, torque references are sent to the robot.

\mathbf{v}_B^{ref} and $\boldsymbol{\omega}_B^{ref}$ of the base and the state of the robot.

C. Motion Optimizer

The motion optimizer generates operational space references for the x , y and z coordinates of the whole-body center of mass (COM) given the support polygon sequence and the robot state [10]. The resulting nonlinear optimization framework is described in the following sections.

1) *Motion plan parameterization*: As described in [10], the x , y , and z coordinates of the COM trajectory are parametrized as a sequence of quintic splines, i.e., the position, velocity and acceleration of the COM are given by $\mathbf{p}_{COM} = \mathbf{T}(t)\boldsymbol{\alpha}_k \in \mathbb{R}^3$, $\dot{\mathbf{p}}_{COM} = \dot{\mathbf{T}}(t)\boldsymbol{\alpha}_k \in \mathbb{R}^3$, and $\ddot{\mathbf{p}}_{COM} = \ddot{\mathbf{T}}(t)\boldsymbol{\alpha}_k \in \mathbb{R}^3$, with $\mathbf{T}(t) = \text{diag}(\boldsymbol{\eta}^T(t), \boldsymbol{\eta}^T(t), \boldsymbol{\eta}^T(t)) \in \mathbb{R}^{3 \times 18}$, $\boldsymbol{\eta}^T(t) = [t^5 \ t^4 \ t^3 \ t^2 \ t \ 1]$, $t \in [\bar{t}, \bar{t} + \Delta t_k]$, where \bar{t} is the sum of time durations of all previous splines, and Δt_k is the time duration of the k -th spline. All coefficients of spline i are stored in $\boldsymbol{\alpha}_k = [\boldsymbol{\alpha}_k^x \ \boldsymbol{\alpha}_k^y \ \boldsymbol{\alpha}_k^z]^T \in \mathbb{R}^{18}$. Finally, we solve for the vector of optimization parameters which is obtained by stacking together all spline coefficient vectors $\boldsymbol{\alpha}_k$.

2) *Optimization problem*: As depicted in Fig. 3, the motion optimization problem can be expressed as a nonlinear optimization problem with objective $f(\boldsymbol{\xi})$ subject to equality constraints $\mathbf{c}(\boldsymbol{\xi}) = \mathbf{0}$ and inequality constraints $\mathbf{h}(\boldsymbol{\xi}) \geq \mathbf{0}$, where $\boldsymbol{\xi}$ is the vector of optimization variables given in Section III-C.1. A sequential quadratic programming (SQP) algorithm [19] is used to solve the optimization problem continuously over a time horizon of τ seconds. Table I summarizes each objective and constraint used in this work.

3) *3D ZMP inequality constraint*: To ensure dynamic stability of the planned motions, an inequality constraint on

TABLE I
OVERVIEW OF ALL COSTS AND CONSTRAINTS OF THE MOTION
OPTIMIZATION PROBLEM BASED ON [10].

Type	Task	Purpose
Objective	Minimize COM acceleration	Smooth motions
Objective	Minimize deviation to previous solution $\boldsymbol{\xi}_{prev}$	Smooth motions
Objective	Track a high-level reference trajectory $\boldsymbol{\pi}$ (path regularizer) $\forall \boldsymbol{\xi}$	Reference tracking
Soft constraint (lin.-quad.)	Minimize deviation to initial & final conditions $\forall \boldsymbol{\xi}$	Disturbance rejection & reference tracking
Soft constraint (lin.-quad.)	Limit overshoots $\forall \boldsymbol{\xi}^z$	Avoid kinematic limits of legs
Constraint (lin. eq.)	Junction constraints \forall pairs of adjacent splines $k, k+1 \forall \boldsymbol{\xi}$	Continuity
Constraint (lin. ineq.)	Push Contact Constraints	Legs can only push the ground
Constraint (nonlin. ineq.)	ZMP criterion	Stability
Soft constraint (nonlin.)	Soften initial ZMP constraints	Relaxation

the ZMP position $\mathbf{p}_{ZMP} \in \mathbb{R}^3$ is included in the motion optimization, where $\mathbf{p}_{ZMP} = \mathbf{n} \times \mathbf{m}_O^{gi} / (\mathbf{n}^T \mathbf{f}^{gi})$ [20]. Here, $\mathbf{m}_O^{gi} \in \mathbb{R}^3$ and $\mathbf{f}^{gi} \in \mathbb{R}^3$ are the components of the *gravito-inertial* wrench [21], with $\mathbf{m}_O^{gi} = m \cdot \mathbf{p}_{ZMP} \times (\mathbf{g} - \ddot{\mathbf{p}}_{ZMP}) - \dot{\mathbf{l}}$ and $\mathbf{f}^{gi} = m \cdot (\mathbf{g} - \ddot{\mathbf{p}}_{ZMP})$, where m is the mass of the robot, \mathbf{l} is the angular momentum of the COM, and \mathbf{g} is the gravity vector. Fig. 2 shows a sketch of the gravito-inertial wrench acting at the COM. As in [10], we assume that $\dot{\mathbf{l}} = \mathbf{0}$.

As illustrated in Fig. 2, the ZMP position \mathbf{p}_{ZMP} is constrained to always lie inside the support polygon. This stability criterion can be formulated as a nonlinear inequality constraint given by [10]

$$[p \ q \ 0] \mathbf{p}_{ZMP} + r \geq 0, \quad (4)$$

where $\mathbf{d} = [p \ q \ r]^T$ describes the edge of a support polygon.

4) *Deformation of support polygons while driving*: In contrast to point feet, the contact locations, and therefore footholds, are not stationary while driving. The support polygon sequence which is needed to fulfill the inequality constraint in (4) is deformed over time. For this purpose, we assume that the number of edges stays constant and therefore, one spline is used to describe the motion of the COM.

First, the expected foothold position for the optimization horizon τ is computed as a function of the reference velocities \mathbf{v}_B^{ref} and $\boldsymbol{\omega}_B^{ref}$. The reference velocities are assumed to be constant over the optimization horizon. Using the time-integrated Rodriguez's formula, the expected foothold position $\mathbf{p}_{\tau,i} \in \mathbb{R}^3$ of leg i is computed by

$$\mathbf{p}_{\tau,i} = \mathbf{p}_{0,i} + \mathbf{R}(\tau \boldsymbol{\omega}_B^{ref}) \frac{1}{\omega_{B,z}^{ref}} \begin{bmatrix} \sin(\omega_{B,z}^{ref} \tau) & -1 + \cos(\omega_{B,z}^{ref} \tau) & 0 \\ 1 - \cos(\omega_{B,z}^{ref} \tau) & \sin(\omega_{B,z}^{ref} \tau) & 0 \\ 0 & 0 & 0 \end{bmatrix} \mathbf{v}_B^{ref}, \quad (5)$$

where $\mathbf{p}_{0,i} \in \mathbb{R}^3$ is the current foothold position. If $\omega_{B,z}^{ref} \approx 0$, the solution becomes $\mathbf{p}_{\tau,i} = \mathbf{p}_{0,i} + \tau \mathbf{v}_B^{ref}$.

Given the coefficients which describe an edge that belongs to the current and expected support polygon, i.e., $\mathbf{d}_0 \in \mathbb{R}^3$ and $\mathbf{d}_\tau \in \mathbb{R}^3$, the deformed edge coefficient vector $\mathbf{d}_k(t)$ at time t is given by interpolation, i.e.,

$$\mathbf{d}(t) = (1 - \frac{t - \bar{t}}{\tau}) \mathbf{d}_\tau + \frac{t - \bar{t}}{\tau} \mathbf{d}_0. \quad (6)$$

IV. WHOLE-BODY CONTROLLER

The operational space reference trajectories of the COM and end-effectors are tracked by a WBC which is based on the hierarchical optimization (HO) framework described in [10], [18]. We optimize over the desired joint accelerations and contact forces which are described by the vector of optimization variables $\boldsymbol{\xi}_d = [\dot{\mathbf{u}}_d^T \ \boldsymbol{\lambda}_d^T]^T \in \mathbb{R}^{n_u \times 3n_c}$, where all symbols are described in Section II.

The WBC is formulated as a QP problem composed of linear equality and inequality tasks, which are solved in a strict prioritized order [22]. The highlighted tasks in Table II are specifically tailored for wheeled-legged robots, and the following sections describe each of these tasks in more detail.

TABLE II

THE TABLE SHOWS A LIST OF PRIORITIZED TASKS (PRIORITY 1 IS THE HIGHEST) USED IN THE WBC. BOLD TASKS ARE TAILORED FOR WHEELED-LEGGED ROBOTS.

Priority	Task
1	Floating base equations of motion Torque limits Friction cone Nonholonomic rolling constraint
2	COM linear motion tracking COM angular motion tracking Swing leg motion tracking Swing wheel rotation minimization Ground leg motion tracking

For the remaining tasks, we rely on the same implementation as used for traditional legged robots [18].

Nonholonomic rolling constraint: The solution found by the optimization needs to take into account the nonholonomic rolling constraint (3). This can be expressed as an equality constraint given by

$$[\mathbf{J}_S \quad \mathbf{0}_{3n_c \times 3n_c}] \boldsymbol{\xi}_d = -\dot{\mathbf{J}}_S \mathbf{u} + [I \ddot{\mathbf{r}}_{IC_1}^T \quad \dots \quad I \ddot{\mathbf{r}}_{IC_{n_c}}^T]^T. \quad (7)$$

Swing leg motion tracking: Given $P\mathbf{r}_{IC_i}^d$, $P\dot{\mathbf{r}}_{IC_i}^d$, and $P\ddot{\mathbf{r}}_{IC_i}^d$, the motion tracking task of each swing leg i is formulated by

$$[\mathbf{J}_{C_i} \quad \mathbf{0}_{3n_c \times 3n_c}] \boldsymbol{\xi}_d = \mathbf{R}_{IP}(P\ddot{\mathbf{r}}_{IC_i}^d + \mathbf{K}_p(P\mathbf{r}_{IC_i}^d - P\mathbf{r}_{IC_i}') + \mathbf{K}_d(P\dot{\mathbf{r}}_{IC_i}^d - P\dot{\mathbf{r}}_{IC_i}')) - \dot{\mathbf{J}}_{C_i} \mathbf{u}, \quad (8)$$

where $\mathbf{K}_p, \mathbf{K}_d \in \mathbb{R}^{3 \times 3}$ are diagonal positive definite matrices which define proportional and derivative gains. Note that all measured values, i.e., \mathbf{J}_{C_i} , $P\mathbf{r}_{IC_i}'$, and $P\dot{\mathbf{r}}_{IC_i}'$, are independent of the wheel angle θ (as discussed in the footnotes of Section II-A).

Swing wheel rotation minimization: For each swing leg i , the wheel's rotation is dampened by adding the task

$$[\mathbf{S}_{W_i} \quad \mathbf{0}_{3n_c \times 3n_c}] \boldsymbol{\xi}_d = -k_d \dot{\theta}_i, \quad (9)$$

where $\mathbf{S}_{W_i} \in \mathbb{R}^{3n_c \times n_u}$ is a matrix which selects the row of $\boldsymbol{\xi}_d$ containing the wheel of leg i , $k_d \in \mathbb{R}$ is a derivative gain, and $\dot{\theta}_i$ is the wheel's rotational speed.

Ground leg motion tracking: To track the desired motion of the grounded legs, we constrain the accelerations in the direction of the rolling direction \mathbf{c}_x . Given the desired motions of the leg-fixed contact point $P\mathbf{r}_{IC_i}^d$, $P\dot{\mathbf{r}}_{IC_i}^d$, and $P\ddot{\mathbf{r}}_{IC_i}^d$, the motion tracking task of each ground leg i is formulated by

$$\pi_{\mathbf{c}_x}([\mathbf{J}_{C_i} \quad \mathbf{0}_{3n_c \times 3n_c}] \boldsymbol{\xi}_d) = \pi_{\mathbf{c}_x}(\mathbf{R}_{IP}(P\ddot{\mathbf{r}}_{IC_i}^d + \mathbf{K}_p(P\mathbf{r}_{IC_i}^d - P\mathbf{r}_{IC_i}') + \mathbf{K}_d(P\dot{\mathbf{r}}_{IC_i}^d - P\dot{\mathbf{r}}_{IC_i}')) - \dot{\mathbf{J}}_{C_i} \mathbf{u}), \quad (10)$$

where $\pi_{\mathbf{c}_x}(\mathbf{a})$ is the projection of a vector \mathbf{a} onto the vector \mathbf{c}_x .

Given the optimal solution $\boldsymbol{\xi}^*$, the desired generalized torques $\boldsymbol{\tau}_d$, which are sent to the robot, are computed by

$$\boldsymbol{\tau}_d = \mathbf{M}_j(\mathbf{q})\dot{\mathbf{u}}^* + \mathbf{h}_j(\mathbf{q}, \mathbf{u}) - \mathbf{J}_{S_j}^T \boldsymbol{\lambda}^*, \quad (11)$$

where $\mathbf{M}_j(\mathbf{q})$, $\mathbf{h}_j(\mathbf{q}, \mathbf{u})$, and \mathbf{J}_{S_j} are the lower rows of the equations of motion in (11) relative to the actuated joints.

V. EXPERIMENTAL RESULTS AND DISCUSSION

In this section, we verify our approach on a real quadrupedal robot equipped with non-steerable, torque-controlled wheels as end-effectors. The robot is driven using external velocity inputs coming from a joystick. All computation was carried out by the PC (Intel i7-5600U, 2.6 - 3.2GHz, dual-core 64-bit) integrated into the robot. A video⁶ showing the results accompanies this paper.

The WBC runs together with state estimation in a 400 Hz loop. A novel state estimation algorithm based on [23] is used to generate an estimation of the robot's position, velocity, and orientation w.r.t. an inertial coordinate frame. Similar to [24], we fuse data from an inertial measurement unit (IMU) as well as the kinematic measurements from each actuator (including the wheels) to acquire a fast state estimation of the robot. The open-source Rigid Body Dynamics Library [25] (RBDL) is used for modeling and computation of kinematics and dynamics based on the algorithms described in [26]. We use a custom SQP algorithm to solve the nonlinear optimization problem in Section III-C.2, which solves the nonlinear problem by iterating through a sequence of QP problems. Each QP problem is solved using QuadProg++ [27] which uses the Goldfarb-Idnani active-set method [28]. Depending on the gait, the motion optimization in Section III-C runs between 100 and 200 Hz.

A. Indoor Environment: Flat Terrain

We performed driving and walking locomotion in an indoor environment, and the results are shown in Fig. 4. The three-dimensional plot shows the measured trajectories of the front legs, hind legs, and the COM. In addition, the zoomed-in plot depicts the transitions between driving and walking in a corner. As discussed in [29], the robot is able to drive

⁶Available at <https://youtu.be/nGLUsyx9Vvc>

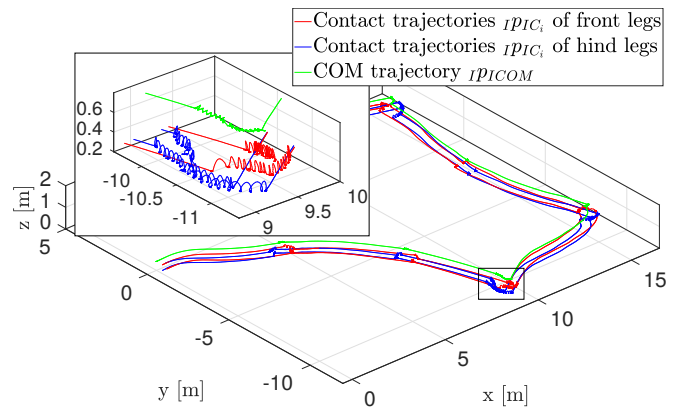


Fig. 4. The robot ANYmal is driving and walking in an indoor environment. The three-dimensional plot shows the operational space, estimated measurements of the robot where the red, blue and green lines depict the contact trajectories of the front legs, the contact trajectories of the hind legs, and the COM trajectories w.r.t. to the inertial frame I . The zoomed-in figure shows transitions between driving and walking. Moreover, the robot is turning in a corner by performing walking motions.

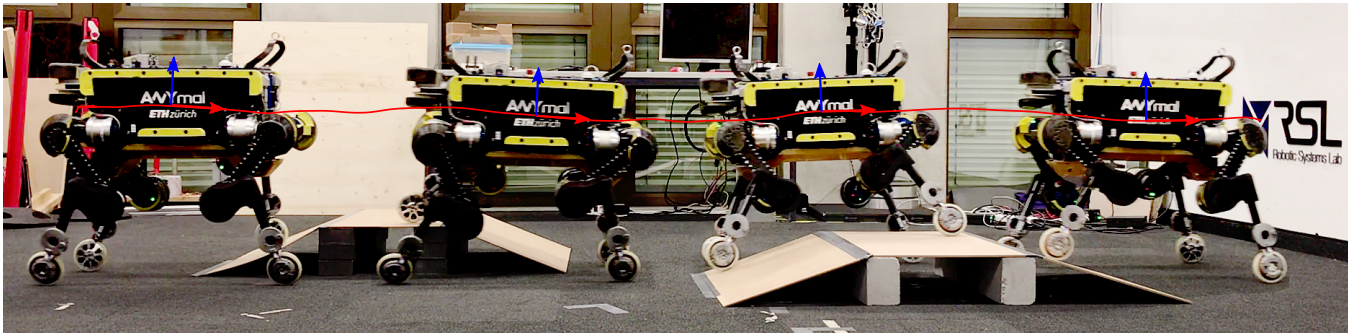


Fig. 5. The robot ANYmal drives over two inclines with a height of approximately 30% of ANYmal’s leg length and the red line depicts the COM trajectory. The maximum speed of the robot is 0.7 m/s.

small curvatures although the robot is equipped with non-steerable wheels. By yawing the base of the robot, the wheels are turning w.r.t. to an inertial frame. For larger curvatures, the robot needs to step. The results successfully prove the omnidirectional capabilities of the robot.

B. Indoor Environment: Inclined Terrain

Fig. 5 depicts the COM motion tracked by the controller while ANYmal is driving blindly over two inclines. This experiment demonstrates the advantage of using torque control. The robot adapts naturally to the unseen terrain irregularities while maintaining the COM height. Moreover, the COM motion is unaffected by the two obstacles although the robot drives at a speed of 0.7 m/s. In addition, none of the wheels violates the friction constraints related to the no-slip condition.

C. Outdoor Environment: Crossing a Street

We conducted an outdoor experiment where we validated the performance of the robot under real-world conditions. Since the robot is able to drive fast and efficiently while being able to overcome obstacles, it is applicable to real-world tasks such as payload delivery. For this purpose, we conducted an experiment where the robot’s task is to cross a street. As can be seen in Fig. 6, the robot is able to drive down a step and to walk over another one. In addition, one of the images shows how the robot rotates its base around the yaw direction to change its driving direction. This experiment also highlights the significant advantages of wheeled-legged robots compared to traditional walking robots. The robot is able to drive down steps with 1 m/s without the need of terrain perception. This advantage is also confirmed by the result in the lower right image of Fig. 6 where the robot drives down a stair without the need to step.

D. High Speed and Low Cost of Transport

We calculated the mechanical cost of transport (COT) while driving on flat terrain based on the calculation in [29]. The robot achieves a COT of 0.25 while driving 2 m/s and the mechanical power consumption is 161.99 W. A comparison to traditional walking [29] shows that the COT is drastically lower for driving. In addition, with 2 m/s we broke ANYmal’s maximum speed record of 1.5 m/s given in [30]. However, this is an expected result, and we expect that

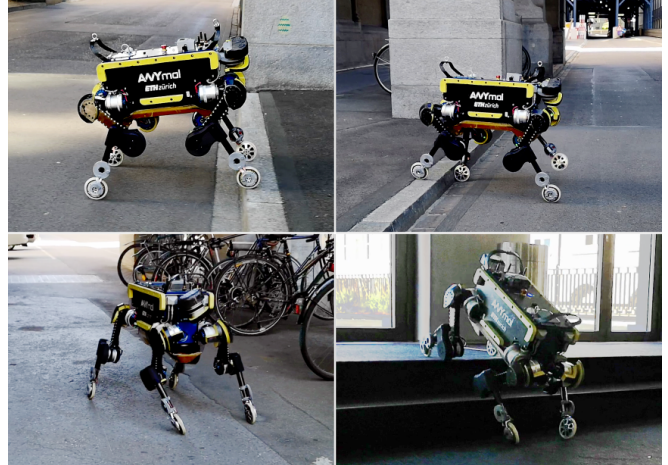


Fig. 6. The figure shows several skills of the wheeled version of ANYmal: dynamically driving down a step with 1 m/s (top left image), walking up a step (top right image), driving in a curve by yawing the base (lower left image), and dynamically driving downstairs with 1 m/s (lower right image).

the robot is able to drive faster since the wheels only reached half of their maximum torque limit during this test.

VI. CONCLUSIONS

In this work, we show a whole-body motion control and planning framework for a quadrupedal robot equipped with non-steerable, torque-controlled wheels as end-effectors. The mobile platform combines the advantages of legged and wheeled robots. In contrast to other wheeled-legged robots, we show for the first time dynamic motions on flat, inclined and rough terrains. These are enabled thanks to the tight integration of the wheels into the motion planning and control framework. For the motion optimization, we rely on a 3D ZMP approach which updates the motion plan continuously. This motion plan is tracked by a hierarchical WBC which considers the nonholonomic contact constraint introduced by the wheels. Thanks to torque control, the robot does not violate the contact constraints, and the fast update rates of the motion control and planning framework make the robot robust against unpredicted terrain irregularities.

We aim to further show the applicability of the system to real-world tasks by conducting more outdoor experiments. Future work will focus on hybrid locomotion strategies, i.e., walking and driving at the same time. In addition, perceptive motion planning over a long time horizon in challenging

environments is still an unsolved problem for wheeled-legged robots (and traditional legged robots).

ACKNOWLEDGMENT

The authors would like to thank Vassilios Tsounis for his support during the development of the wheel actuator firmware. Furthermore, our gratitude goes to Francisco Giráldez Gámez and Christian Gehring who helped with the preliminary investigation of the rolling constraint.

REFERENCES

- [1] C. D. Bellicoso, M. Bjelonic, L. Wellhausen, K. Holtmann, F. Günther, M. Tranzatto, P. Fankhauser, and M. Hutter, "Advances in real-world applications for legged robots," *under review for Journal of Field Robotics*, 2018.
- [2] M. Hutter, C. Gehring, D. Jud, A. Lauber, C. D. Bellicoso, V. Tsounis, J. Hwangbo, K. Bodie, P. Fankhauser, M. Bloesch, *et al.*, "ANYmal - a highly mobile and dynamic quadrupedal robot," in *IEEE/RSJ International Conference on Intelligent Robots and Systems (IROS)*, 2016.
- [3] W. Reid, F. J. Pérez-Grau, A. H. Göktoğan, and S. Sukkarieh, "Actively articulated suspension for a wheel-on-leg rover operating on a martian analog surface," in *IEEE International Conference on Robotics and Automation (ICRA)*, 2016.
- [4] P. R. Giordano, M. Fuchs, A. Albu-Schaffer, and G. Hirzinger, "On the kinematic modeling and control of a mobile platform equipped with steering wheels and movable legs," in *IEEE International Conference on Robotics and Automation*, 2009.
- [5] F. Cordes, C. Oekermann, A. Babu, D. Kuehn, T. Stark, F. Kirchner, and D. R. I. C. Bremen, "An active suspension system for a planetary rover," in *Proceedings of the International Symposium on Artificial Intelligence, Robotics and Automation in Space*, 2014.
- [6] M. Gifthalder, F. Farshidian, T. Sandy, L. Stadelmann, and J. Buchli, "Efficient kinematic planning for mobile manipulators with non-holonomic constraints using optimal control," in *IEEE International Conference on Robotics and Automation (ICRA)*, 2017.
- [7] J. Lim, I. Lee, I. Shim, H. Jung, H. M. Joe, H. Bae, O. Sim, J. Oh, T. Jung, S. Shin, *et al.*, "Robot system of DRC-HUBO+ and control strategy of team kaist in darpa robotics challenge finals," *Journal of Field Robotics*, 2017.
- [8] T. Klamt and S. Behnke, "Anytime hybrid driving-stepping locomotion planning," in *Int. Conference on Intelligent Robots and Systems (IROS)*, 2017.
- [9] Centauro-Project. Centauro robot publications. Centauro-Project. [Online]. Available: <https://www.centauro-project.eu/publications>
- [10] C. D. Bellicoso, F. Jenelten, C. Gehring, and M. Hutter, "Dynamic locomotion through online nonlinear motion optimization for quadrupedal robots," *IEEE Robotics and Automation Letters*, 2018.
- [11] J. Pratt, P. Dilworth, and G. Pratt, "Virtual model control of a bipedal walking robot," in *IEEE International Conference on Robotics and Automation (ICRA)*, 1997.
- [12] C. Gehring, S. Coros, M. Hutler, C. D. Bellicoso, H. Heijnen, R. Diethelm, M. Bloesch, P. Fankhauser, J. Hwangbo, M. Hoepflinger, *et al.*, "Practice makes perfect: An optimization-based approach to controlling agile motions for a quadruped robot," *IEEE Robotics & Automation Magazine*, 2016.
- [13] G. Bledt, P. M. Wensing, and S. Kim, "Policy-regularized model predictive control to stabilize diverse quadrupedal gaits for the mit cheetah," in *IEEE/RSJ International Conference on Intelligent Robots and Systems (IROS)*, 2017.
- [14] H.-W. Park, P. M. Wensing, and S. Kim, "High-speed bounding with the mit cheetah 2: Control design and experiments," *The International Journal of Robotics Research*, 2017.
- [15] A. W. Winkler, C. D. Bellicoso, M. Hutter, and J. Buchli, "Gait and trajectory optimization for legged systems through phase-based end-effector parameterization," *IEEE Robotics and Automation Letters*, 2018.
- [16] Boston Dynamics. Introducing handle. Youtube. [Online]. Available: <https://www.youtube.com/watch?v=-7xvqQeoA8c>
- [17] M. Vukobratović and B. Borovac, "Zero-moment point thirty five years of its life," *International journal of humanoid robotics*, 2004.
- [18] C. D. Bellicoso, F. Jenelten, P. Fankhauser, C. Gehring, J. Hwangbo, and M. Hutter, "Dynamic locomotion and whole-body control for quadrupedal robots," in *IEEE/RSJ International Conference on Intelligent Robots and Systems (IROS)*, 2017.
- [19] P. T. Boggs and J. W. Tolle, "Sequential quadratic programming," *Acta numerica*, 1995.
- [20] P. Sardain and G. Bessonnet, "Forces acting on a biped robot. center of pressure-zero moment point," *IEEE Transactions on Systems, Man, and Cybernetics-Part A: Systems and Humans*, 2004.
- [21] S. Caron, Q.-C. Pham, and Y. Nakamura, "Zmp support areas for multicontact mobility under frictional constraints," *IEEE Transactions on Robotics*, 2017.
- [22] C. D. Bellicoso, C. Gehring, J. Hwangbo, P. Fankhauser, and M. Hutter, "Perception-less terrain adaptation through whole body control and hierarchical optimization," in *Humanoid Robots (Humanoids), 2016 IEEE-RAS 16th International Conference on*. IEEE, 2016, pp. 558–564.
- [23] M. Bloesch, M. Burri, H. Sommer, R. Siegwart, and M. Hutter, "The two-state implicit filter recursive estimation for mobile robots," *IEEE Robotics and Automation Letters*, 2018.
- [24] M. Bloesch, M. Hutter, M. A. Hoepflinger, S. Leutenegger, C. Gehring, C. D. Remy, and R. Siegwart, "State estimation for legged robots-consistent fusion of leg kinematics and imu," *Robotics*, 2013.
- [25] M. Felis. Rigid Body Dynamics Library. [Online]. Available: <https://bitbucket.org/rbd/rbd/src/default/>
- [26] R. Featherstone, *Rigid body dynamics algorithms*. Springer, 2014.
- [27] L. D. Gasper. QuadProg++. [Online]. Available: <http://quadprog.sourceforge.net/>
- [28] D. Goldfarb and A. Idnani, "A numerically stable dual method for solving strictly convex quadratic programs," *Mathematical programming*, 1983.
- [29] M. Bjelonic, C. D. Bellicoso, M. E. Tiryaki, and M. Hutter, "Skating with a force controlled quadrupedal robot," in *IEEE/RSJ International Conference on Intelligent Robots and Systems (IROS 2018)*, 2018.
- [30] J. Hwangbo, J. Lee, A. Dosovitskiy, D. Bellicoso, V. Tsounis, V. Koltun, and M. Hutter, "Learning agile and dynamic motor skills for legged robots," *under review for Science Robotics*, 2018.